

A novel model-marginalized cosmological bound on the QCD axion mass

Eleonora Di Valentino,^{1,*} Stefano Gariazzo,^{2,†} William Giarè,^{3,4,‡}
Alessandro Melchiorri,^{5,§} Olga Mena,^{6,¶} and Fabrizio Renzi^{7,**}

¹*School of Mathematics and Statistics, University of Sheffield,
Hounsfield Road, Sheffield S3 7RH, United Kingdom*

²*Istituto Nazionale di Fisica Nucleare (INFN), Sezione di Torino, Via P. Giuria 1, I-10125 Turin, Italy*

³*Galileo Galilei Institute for theoretical physics, Centro Nazionale INFN di Studi Avanzati,
Largo Enrico Fermi 2, I-50125, Firenze, Italy*

⁴*INFN Sezione di Roma, P.le A. Moro 2, I-00185, Roma, Italy*

⁵*Physics Department and INFN, Università di Roma “La Sapienza”, P.le Aldo Moro 2, 00185, Rome, Italy*

⁶*Instituto de Física Corpuscular (CSIC-Universitat de València), E-46980 Paterna, Spain*

⁷*Lorentz Institute for Theoretical Physics, Leiden University,
PO Box 9506, Leiden 2300 RA, The Netherlands*

(Dated: May 26, 2023)

We present model-marginalized limits on mixed hot dark matter scenarios, which consider both thermal neutrinos and thermal QCD axions. A novel aspect of our analyses is the inclusion of small-scale Cosmic Microwave Background (CMB) observations from the Atacama Cosmology Telescope (ACT) and the South Pole Telescope (SPT), together with those from the Planck satellite and Baryon Acoustic Oscillation (BAO) data. After marginalizing over a number of well-motivated non-minimal background cosmologies, the tightest 95% CL upper bound we obtain is 0.21 eV, both for $\sum m_\nu$ and m_a , from the combination of ACT, Planck and BAO measurements. Restricting the analyses to the standard Λ CDM picture, we find $\sum m_\nu < 0.16$ eV and $m_a < 0.18$ eV, both at 95% CL. Interestingly, the best background cosmology is never found within the minimal Λ CDM plus hot relics, regardless of the data sets exploited in the analyses. The combination of Planck with either BAO, SPT or ACT prefers a universe with a non-zero value of the running in the primordial power spectrum with strong evidence. Small-scale CMB probes, both alone and combined with BAO, either prefer, with substantial evidence, non-flat universes (as in the case of SPT) or a model with a time varying dark energy component (as in the case of ACT).

Keywords: Axions

I. INTRODUCTION

The Peccei-Quinn (PQ) mechanism [1, 2] represents the most elegant solution to the strong CP problem in Quantum Chromodynamics [3–5]. The key ingredient consists of a new dynamical pseudo-scalar field – the *axion* [6, 7] – which is driven towards its minimal energy configuration by the QCD dynamics, restoring the CP-invariance of strong interactions [8].

The implications of a cosmic axion background crucially depend on the underlying production mechanism [9]. If axions are produced via non-thermal channels, (*e.g.* by the vacuum realignment mechanism [10–16] and/or by topological defects decay [17–24]) they should be considered natural cold dark matter candidates [10–12].

Conversely, a thermal population of axions produced by scattering and decays of particles can provide additional radiation energy-density contributing to the hot

dark matter component of the Universe, similarly to massive neutrinos. Notice also that, while the axion cold dark matter density is a decreasing function of the mass, the axion couplings are proportional to the mass itself. In order to have a significant thermal population, axions must represent a sub-dominant component of the total cold dark matter abundance and these two scenarios can be analyzed separately.

In this work we shall focus on the thermal axion mass limits from cosmology. A mandatory first step is the calculation of the axion relic abundance.

While most of the cosmological analyses carried out in the literature [25–35] have been based on chiral perturbation theory, in Ref. [36] it was pointed out that this approach can be safely extended only up to a temperature $T \lesssim 60$ MeV (see also Ref. [37, 38]), since the perturbative scheme breaks down. A practical solution to settle this issue employs an interpolation of the thermalization rate to cover the gap between the highest safe temperature reachable by chiral perturbation theory and the regime above the confinement scale, where the axion production rate is instead dominated by the axion-gluon scattering [39, 40]. Improved cosmological bounds [41] have been derived for two traditional benchmark models of QCD axion interactions namely, the KSVZ [42, 43]

* e.divalentino@sheffield.ac.uk

† gariazzo@to.infn.it

‡ william.giare@uniroma1.it

§ alessandro.melchiorri@roma1.infn.it

¶ omena@ific.uv.es

** renzi@lorentz.leidenuniv.nl

and the DFSZ one [44, 45] (see also Ref. [46]).¹ As discussed in the same Ref. [41], the choice between KSVZ and DFSZ axion interaction scenarios does not result in a significant difference in the cosmological constraint on the axion mass, so that the current 95% CL upper limits obtained in mixed hot dark matter scenarios in which massive neutrino species are also considered are $m_a \lesssim 0.2$ eV and $\sum m_\nu \lesssim 0.15$ eV [41], using the most recent Cosmic Microwave Background (CMB) data released by the *Planck* satellite [51–54], the astrophysical observations of primordial light elements forged during the Big Bang Nucleosynthesis (BBN) epoch [52, 55–57], and the large scale structure information of the Universe in the form of Baryon Acoustic Oscillation (BAO) measurements [58–60], see also the recent [61, 62].

However, these limits have been obtained under two *standardized* assumptions in cosmological parameter analyses. Namely, (1) that the underlying model describing our universe is the minimal flat Λ CDM, and, (2) restricting CMB measurements to those from the *Planck* satellite observations. Concerning the first assumption, one should realize that a number of several intriguing tensions and anomalies have emerged at different statistical levels [63–66], questioning the validity of the canonical flat Λ CDM picture. A small curvature component, or a more general dark energy fluid, are some examples of very promising scenarios that should be carefully explored. From what regards the second assumption, analyses should also include the recent small-scale measurements of the CMB angular power spectra released by the Atacama Cosmology Telescope [67, 68] (ACT) and the South Pole Telescope [69, 70] (SPT) Collaborations. It is therefore clear that the role of parameterizations, priors and models may lead to different constraints on the cosmological neutrino and axion masses.

Quantifying the impact resulting from the parameterization adopted for the cosmological model [71, 72] and also from including independent CMB observations [73, 74] is the main goal of the present study, where, focusing exclusively on the KSVZ axion model, we derive new model-marginalized limits on hot dark matter scenarios involving axions & massive neutrinos.

The paper is organized as follows: in [section II](#) we explain our statistical, computational and data analysis methods, in [section III](#) we present the bounds on the hot dark matter masses in the different cosmological scenarios, together with the model-marginalized limits. We conclude in [section IV](#).

II. METHODOLOGY

A. Bayesian statistics

The first aim of this study is to test how the results change when an extended cosmological model is considered as the underlying theory, instead of the simple Λ CDM scenario. In order to do that, we proceed by performing a marginalization over a number of different models.²

Given a set of models (\mathcal{M}_i), in order to compute the model-marginalized posterior, one starts defining the posterior probabilities, p_i , of the model \mathcal{M}_i over all the possible models:

$$p_i = \frac{\pi_i Z_i}{\sum_j \pi_j Z_j}, \quad (1)$$

where π_i and Z_i indicates the prior probability and the Bayesian evidence of model \mathcal{M}_i . The model-marginalized posterior $p(\theta|d)$ for a set of parameters θ , given some data d , reads as

$$p(\theta|d) \equiv \sum_i p(\theta|d, \mathcal{M}_i) p_i, \quad (2)$$

where $p(\theta|d, \mathcal{M}_i)$ is the parameter posterior within the model \mathcal{M}_i . If all models have the same prior and using the Bayes factors $B_{i0} = Z_i/Z_0$ with respect to the favored model \mathcal{M}_0 , the model-marginalized posterior is:

$$p(\theta|d) = \frac{\sum_i p(\theta|d, \mathcal{M}_i) B_{i0}}{\sum_j B_{j0}}. \quad (3)$$

Notice that if the Bayes factors are large in favor of the simplest and usually preferred model, extensions of the minimal picture will not contribute significantly to the model-marginalized posterior. In order to perform Bayesian model comparison using the Bayes factors and evaluate the strength of preference in favor of the best model, we follow a modified version of the Jeffreys' scale³ extracted from Ref. [76], see [Table I](#).

At the time of determining neutrino mass bounds, since the likelihood cannot put lower limits on the neutrino masses, the prior range and shape can play a significant role, as discussed for example in [71, 77–79]. In order to avoid the dependency on prior in determining credible intervals, another possibility is to adopt the method of

¹ Although the KSVZ and DFSZ axion models are widely recognized as the most popular benchmark models [47, 48], it is worth considering numerous alternative models as well. Recent developments in this area can be found in Refs.[49, 50]. For a comprehensive review of these models, we refer to Ref.[9].

² We would like to emphasize that our approach is to let the data determine whether a model is favored or disfavored, without introducing any pre-existing knowledge, based on both theoretical arguments or different observations, that could bias the results. This is to respect the principle that the theory should be informed by the data and not the other way around, and therefore we consider our approach to be both fair and conservative.

³ Notice that our empirical scale, summarized [Table I](#), deviates from the scale defined in the original Jeffreys' work [75])

$ \ln B_0 $	Odds	Probability	Strength of evidence
< 0.1	$\lesssim 3 : 1$	< 0.750	Inconclusive
1	$\sim 3 : 1$	0.750	Weak
2.5	$\sim 12 : 1$	0.923	Moderate
5	$\sim 150 : 1$	0.993	Strong

Table I: Modified Jeffreys' empirical scale to establish the strength of evidence when comparing two competing models.

Ref. [80]. Given some model \mathcal{M} which contains a parameter x (for instance, the axion or the neutrino mass), the *relative belief updating ratio* $\mathcal{R}(x_1, x_2|d, \mathcal{M})$ is defined as:

$$\mathcal{R}(x_1, x_2|d, \mathcal{M}) \equiv \frac{Z_{\mathcal{M}}^{x_1}}{Z_{\mathcal{M}}^{x_2}}, \quad (4)$$

where $Z_{\mathcal{M}}^x$ is defined as the Bayesian evidence of model \mathcal{M} but fixing x to a specific value:⁴

$$Z_{\mathcal{M}}^x = \int_{\Omega_\psi} d\psi \pi(\psi|\mathcal{M}) \mathcal{L}_{\mathcal{M}}(x, \psi), \quad (5)$$

where ψ represents all the parameters in model \mathcal{M} except x , which can vary in a parameter space Ω_ψ , $\pi(\psi|\mathcal{M})$ is their prior (notice that the x prior is not included here) and \mathcal{L} is the likelihood.

From Eq. (4), we easily understand that the relative belief updating ratio does not represent a probability, as it is the ratio of two evidences. Importantly, the function $\mathcal{R}(x_1, x_2|d, \mathcal{M})$ is completely prior-independent. Using the Bayes theorem, it is possible to obtain a different expression for the former function:

$$\mathcal{R}(x_1, x_2|d, \mathcal{M}) = \frac{p(x_1|d, \mathcal{M})/\pi(x_1|\mathcal{M})}{p(x_2|d, \mathcal{M})/\pi(x_2|\mathcal{M})}, \quad (6)$$

where $\pi(x|\mathcal{M})$ is the unidimensional prior on x . This formulation is extremely useful in Monte Carlo Markov Chain (MCMC) runs where one can calculate these functions directly from the run chains. The definition of $\mathcal{R}(x_1, x_2|d)$ can be easily extended to perform a model marginalization:

$$\mathcal{R}(x_1, x_2|d) \equiv \frac{\sum_i Z_{\mathcal{M}_i}^{x_1} \pi(\mathcal{M}_i)}{\sum_j Z_{\mathcal{M}_j}^{x_2} \pi(\mathcal{M}_j)}, \quad (7)$$

where now the evidences $Z_{\mathcal{M}_j}^x$ are computed within a specific model and $\pi(\mathcal{M}_j)$ is the model prior. In order

to write $\mathcal{R}(x_1, x_2|d)$ using the parameter prior and posterior, the simplest assumption is to consider the same prior $\pi(x)$ within all the models. In such case, Eq. (7) becomes:

$$\mathcal{R}(x_1, x_2|d) = \frac{p(x_1|d)/\pi(x_1)}{p(x_2|d)/\pi(x_2)}, \quad (8)$$

where $p(x|d)$ is the model-marginalized posterior in Eq. (2).

B. Axion Modeling

We address the effects induced by a relic population of thermal axions by employing a modified version of the Boltzmann integrator code CAMB [81, 82]. The code has been modified to accommodate the effects of QCD axions on cosmological scales only in terms of the axion mass which we employ as an additional cosmological parameters in our analysis, see Ref. [41] for a detailed calculation. We vary the axion mass in the range between 0.01 eV and 10 eV and focus exclusively on the KSVZ model of axion-hadron interactions.

As long as the axion remains relativistic ($T_a \gg m_a$), it behaves as radiation in the early Universe and its cosmological effects are those produced via their contribution to the effective number of neutrino species N_{eff} . As detailed in Ref. [41], such a contribution is precisely evaluated by solving the Boltzmann equation for the axion number density in the early Universe. Indeed, very light axions ($m_a \lesssim 0.1$ eV) are still relativistic at recombination and thus modify the CMB angular power spectrum via N_{eff} . While such corrections are typically very small ($\Delta N_{\text{eff}} \sim 0.03$), they are relevant for the next generation of CMB experiments [83]. On the other hand, heavier axions with masses larger than 0.1 eV are highly non-relativistic at the recombination epoch. In this case, their impact on the CMB angular power spectra is both direct (through their impact on the early integrated Sachs-Wolfe effect, similarly to massive neutrinos) and indirect (by modifying the primordial helium abundance during the BBN). In this regard, it is worth stressing that the axion starts behaving as cold dark matter much earlier

⁴ We also assume that the prior on x is independent on the other parameters and viceversa.

than massive neutrinos, leading to a significant impact on structure formation. This feature, not only allows to distinguish massive neutrinos from massive axions through their effect on structure formation but it also allows to set stringent constraints on the axion mass exploiting large scale structure data, as well. Nonetheless, when the two species have similar masses, the evolution of their energy densities prevent to reach constraints on their masses lower than ~ 0.1 eV, see also Refs. [41, 84]. Allowing for a prior on the axion mass spanning three orders of magnitude we can properly take into account all these effect of light and heavy axions on the CMB anisotropies, see Table II.

C. Cosmological Model Parameterization

Parameter	Prior
$\Omega_b h^2$	[0.005, 0.1]
$\Omega_c h^2$	[0.005, 0.1]
Ω_k	[-0.3, 0.3]
w_0	[-3, 1]
w_a	[-3, 2]
$100 \theta_{MC}$	[0.5, 10]
$\log(10^{10} A_s)$	[2.91, 3.91]
n_s	[0.8, 1.2]
α_s	[-1, 1]
$\sum m_\nu$ [eV]	[0.06, 5]
m_a [eV]	[0.01, 10]

Table II: List of uniform prior distributions for cosmological parameters.

As pointed out in the [Introduction](#), a key point in our analysis is to derive robust bounds on the hot dark matter sector marginalizing over a plethora of possible background cosmologies. Therefore, along with the six Λ CDM parameters (the amplitude A_s and the spectral index n_s of scalar perturbations, the baryon $\Omega_b h^2$ and the cold dark matter $\Omega_c h^2$ energy densities, the angular size of the sound horizon at recombination θ_{MC} and the reionization optical depth, τ), we also include the sum of neutrino masses $\sum m_\nu$ and the axion mass m_a . We then explore several extensions of this minimal model, enlarging the parameter space including one or more parameters, such as a running of the scalar index (α_s), a curvature component (Ω_k), and the dark energy equation of state parameters (w_0 and w_a) (see [Table II](#) for the priors adopted in the cosmological parameters).

- The running of scalar spectral index, α_s . In simple inflationary models, the running of the spec-

tral index is a second order perturbation and it is typically very small. However, specific models can produce a large running over a range of scale accessible to CMB experiments. Indeed, a non-zero value of α_s alleviates the $\sim 2.7\sigma$ discrepancy in the value of the scalar spectral index n_s measured by *Planck* ($n_s = 0.9649 \pm 0.0044$) [85, 86] and by the *Atacama Cosmology Telescope* (ACT) ($n_s = 1.008 \pm 0.015$) [68], see Refs. [73, 74, 87].

- Curvature density, Ω_k . Recent data analyses of the CMB temperature and polarization spectra from Planck 2018 team exploiting the baseline *Plik* likelihood suggest that our Universe could have a closed geometry at more than three standard deviations [85, 88–90]. These hints mostly arise from TT observations, that would otherwise show a lensing excess [91–93]. In addition, analyses exploiting the *CamSpec* TT likelihood [94, 95] point to a closed geometry of the Universe with a significance above 99% CL. Furthermore, an indication for a closed universe is also present in the BAO data, using Effective Field Theories of Large Scale Structure [96]. These recent findings strongly motivate to leave the curvature of the Universe as a free parameter [97] and obtain limits on the neutrino and axion masses in this context.
- Dynamical Dark Energy equation of state. Cosmological neutrino and axion mass bounds become weaker if the dark energy equation of state is taken as a free parameter. Even if current data fits well with the assumption of a cosmological constant within the minimal Λ CDM scenario, the question of having an equation of state parameter different from -1 remains certainly open. Along with constant dark energy equation of state models, in this paper we also consider the possibility of having a time-varying $w(a)$ described by the Chevalier-Polarski-Linder parametrization (CPL) [98, 99]:

$$w(a) = w_0 + (1 - a)w_a \quad (9)$$

where a is the scale factor and is $a_0 = 1$ at the present time, $w(a_0) = w_0$ is the value of the equation of state parameter today. Dark energy changes the distance to the CMB consequently pushing it further (closer) if $w < -1$ ($w > -1$) from us. This effect can be balanced by having a larger matter density or, equivalently, by having more massive hot relics, leading to less stringent bounds on both the neutrino and axion masses. Accordingly, the mass bounds of cosmological neutrinos and axions become weaker if the dark energy equation of state is taken as a free parameter.

D. Statistical Analyses and Likelihoods

In order to study the constraints achievable by current CMB and large scale structure probes, we make use of the publicly available code COBAYA [100]. The code explores the posterior distributions of a given parameter space using the Monte Carlo Markov Chain (MCMC) sampler developed for COSMOMC [101] and tailored for parameter spaces with speed hierarchy implementing the "fast dragging" procedure developed in [102]. The prior distributions for the parameters involved in our analysis are chosen to be uniform along the range of variation (see Table II) with the exception of the optical depth for which the prior distribution is chosen accordingly to the CMB datasets as discussed below. To perform model comparison, we compute the Bayesian Evidence of the different models and estimate the Bayes factors through the publicly available package MCEvidence,⁵ properly modified to be compatible with COBAYA.

We verified in some selected cases that the Bayes factors obtained with MCEvidence are similar to those we obtained using PolyChord [105, 106], but much less time-consuming to obtain. We quantified the difference between MCEvidence and PolyChord results by means of a set of dedicated simulations, for which we employed a 3D multi-modal Gaussian likelihood to constrain a 3-parameter model as the simplest case, and compare it with two different models with 4 parameters. The Bayesian evidences obtained with MCEvidence are systematically larger than those obtained with PolyChord by a factor of approximately e . When computing the logarithm of the Bayes factors, the difference between MCEvidence and PolyChord ranges between -0.5 and 0.2 in the cases under consideration. Therefore, we estimate that the values of the logarithms of the Bayes factors reported in the following have an uncertainty of 0.5 with respect to the values that one could have obtained with PolyChord. It is worth noting that the estimation of Bayes factors, starting from the MCMC, is weakly dependent on the chosen priors for cosmological parameters so that adopting uniform priors on $\sum m_\nu$ and m_a may lead to differences in the resulting Bayesian Evidences. The impact of a uniform prior on $\sum m_\nu$ has been extensively discussed in literature, see e.g., Refs. [77, 79, 80, 107–110]. Concerning the axion mass, in our analysis, we focus on the cosmological thermal axion window and set a lower limit of $m_a \gtrsim 0.01$ eV in the prior. This range can be well explored using both linear and logarithmic sampling methods, and we checked that the choice of prior do not significantly affect the resulting limits or Bayesian Evidences.

Concerning the cosmological and astrophysical observations, our baseline data-sets and likelihoods include:

- Planck 2018 temperature and polarization (TT TE EE)

likelihood, which also includes low multipole data ($\ell < 30$) [51–53]. We refer to this combination as "Planck 2018".

- Planck 2018 temperature and polarization (TT TE EE) likelihood up to multipole $\ell = 650$, to use in combination with the alternative ground-based small-scales CMB experiments. We refer to this combination as "Planck650".
- Planck 2018 lensing likelihood [54], reconstructed from measurements of the power spectrum of the lensing potential. We refer to this dataset as "lensing".
- Atacama Cosmology Telescope DR4 temperature and polarization (TT TE EE) likelihood, with a Gaussian prior on the optical depth at reionization $\tau = 0.065 \pm 0.015$, as done in [111]. We refer to this dataset combination as "ACT."
- South Pole Telescope polarization (TE EE) measurements SPT-3G [70] combined with a Gaussian prior on the optical depth at reionization $\tau = 0.065 \pm 0.015$. We refer to this dataset combination as "SPT-3G."
- Baryon Acoustic Oscillations (BAO) measurements extracted from data from the 6dFGS [58], SDSS MGS [59] and BOSS DR12 [60] surveys. We refer to this dataset combination as "BAO".

III. RESULTS

We start by discussing the limits in the mixed hot dark matter scenario assuming the standard Λ CDM cosmology. All the results for this case are provided in Appendix A, Table V. The tightest constraints are obtained when combining Planck650 temperature, polarization and lensing measurements with ACT-CMB and BAO data: the limits we get on the hot dark matter relic masses are $m_a < 0.18$ eV and $m_\nu < 0.16$ eV, both at 95% CL. Adding ACT CMB observations therefore considerably improves the limit on hot relics, as with Planck plus BAO data alone the 95% CL bounds are $m_a < 0.28$ eV and $m_\nu < 0.16$ eV, in perfect agreement with the results for the KSVZ model of Ref. [41] (see also the recent [61]). Concerning the remaining cosmological parameters, notice that both ACT and SPT observations (either alone or combined with BAO) prefer $n_s \simeq 1$, pointing to a Harrison-Zel'dovich primordial power spectrum, as can also be noticed from the left panel of Figure 1 (see also Ref. [87]).

Enlarging the minimal Λ CDM picture with a curvature component Ω_k only degrades mildly the limits on $\sum m_\nu$, while the limit on m_a remains unchanged. From the results provided in Appendix A, Table VI one can notice that the most constraining bounds are $m_a < 0.18$ eV and $m_\nu < 0.20$ eV, both at 95% CL for ACT plus Planck650 plus BAO observations. The preference for $n_s \simeq 1$ from

⁵ github.com/yabebalFantaye/MCEvidence [103, 104].

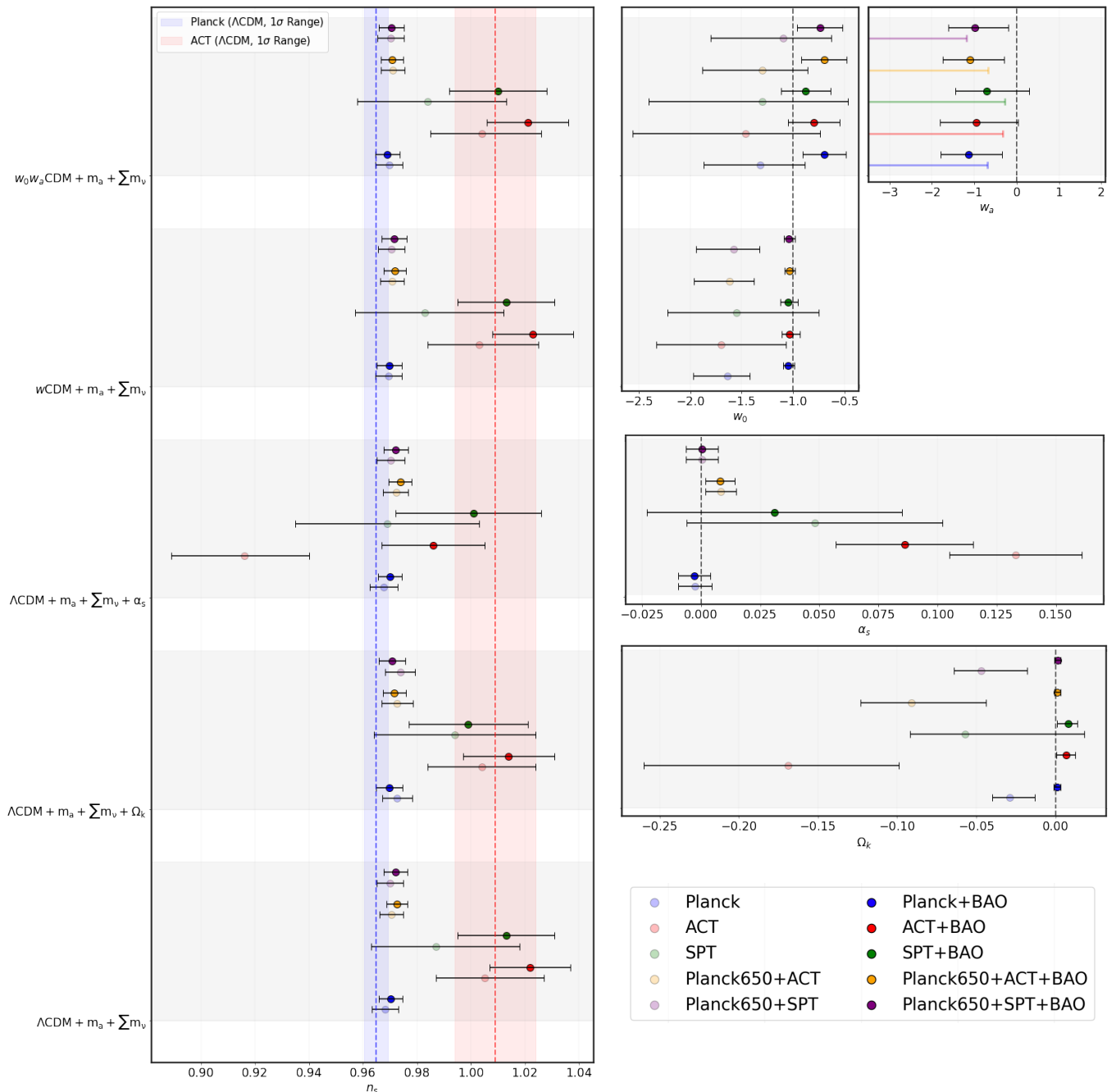


Figure 1: Whisker plot with the mean values and their 68% CL associated errors on n_s , w_0 , w_a , α_s and Ω_k for different data combinations. The darker (lighter) circles depict the CMB limits with (without) the addition of BAO measurements. In the case of n_s (left panel), we show the results for different background cosmologies, and the blue (red) vertical region refers to the value of n_s as measured by Planck (ACT) within the baseline ΛCDM model.

SPT and ACT still persists, see the left panel of Figure 1. Notice that *all* CMB data prefer a value of $\Omega_k < 0$ with a significance above the $\sim 2\sigma$ level for most of the cases. When CMB observations are combined with BAO measurements such a preference is however diluted. This behavior is shown in the bottom right panel of Figure 1.

Including a running (α_s) of the scalar spectral index n_s , the 95% CL bounds for the most powerful data set

combination (i.e. Planck650 plus ACT and BAO) are $m_a < 0.25$ eV and $m_\nu < 0.17$ eV, limiting the constraining power of these observations within the minimal ΛCDM scenario. Interestingly, the preference for $n_s \simeq 1$ from either SPT and/or ACT is not as strong as in the previous two background cosmologies (see the left panel of Figure 1) and it is instead translated into a mild preference for a non-zero value of α_s in the case of SPT.

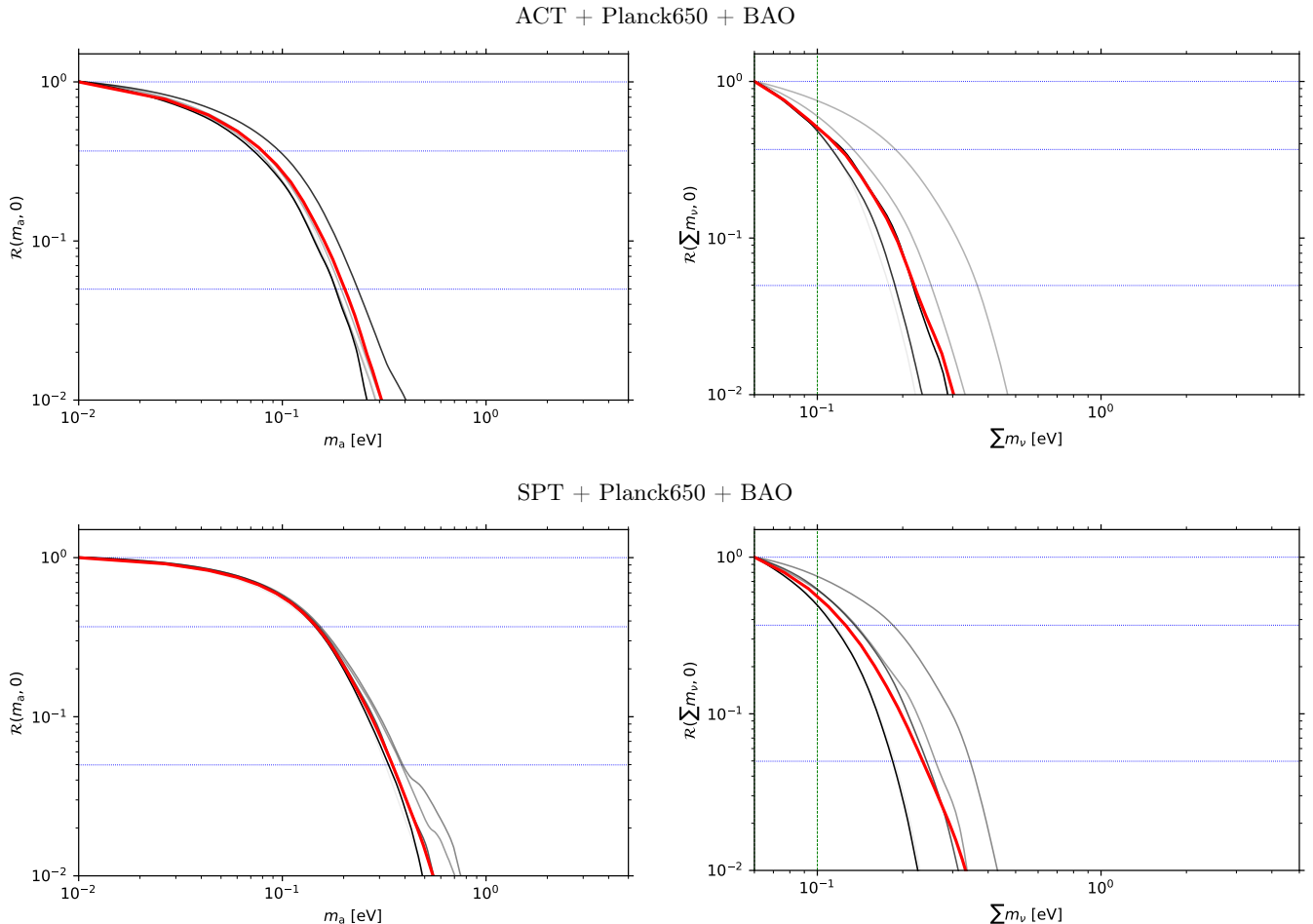


Figure 2: Model-marginalized relative belief updating ratio \mathcal{R} for m_a (left) and $\sum m_\nu$ (right), considering the extensions of the Λ CDM model considered here. Black and gray lines show the \mathcal{R} function within each model, where the darker lines are those that contribute most to the model marginalization, that is, they have the best Bayesian evidences. Horizontal lines show the significance levels $\exp(-1)$ and $\exp(-3)$. The upper (lower) panel refers to the ACT + Planck650 + BAO (SPT + Planck650 + BAO) data analyses. Vertical lines indicate the value 0.1 eV, corresponding to the approximate lower limits for $\sum m_\nu$ in the inverted ordering case.

However, ACT observations shows a $\sim 5\sigma$ preference for a positive value of α_s , see the whisker plot in the right panel of Figure 1, that corresponds to a preference for a positive neutrino mass. All the results for this case are provided in Appendix A, Table VII.

We now leave freedom in the dark sector of the background cosmology. We start by discussing the simplest dark energy model with a constant dark energy equation of state w_0 . The result for this case are provided in Appendix A, Table VIII. First of all, notice that *all* CMB measurements prefer a phantom dark energy universe, that is, a universe in which $w_0 < -1$. The significance is larger than 2σ when considering Planck measurements, either alone or in combination with other CMB data sets. The larger negative value of w_0 is associated to a very large value of H_0 , due to their strong degeneracy. Indeed, it has been shown that a phantom-like dark en-

ergy component can solve the current tension between high-redshift estimates and local universe measurements of the Hubble constant [112]. The addition of BAO observations leads however the value of w_0 very close to its cosmological constant expectation of $w_0 = -1$ and the mean value of the Hubble constant is notably reduced, $H_0 \sim 69$ km/s/Mpc. The results for w_0 are illustrated in the top right panel of Figure 1. Concerning the limits on the hot relic masses, we obtain $m_a < 0.18$ eV for the axion mass and $\sum m_\nu < 0.23$ eV for the neutrino masses, both at 95% CL for the most powerful data set combination, which is, as in the previous background cosmologies, the one exploiting Planck650 plus ACT plus BAO observations. While the axion mass bound barely changes from the standard Λ CDM case, the neutrino mass limit is degraded to $\sum m_\nu < 0.23$ eV, due to the strong degeneracy between the neutrino mass and the dark energy

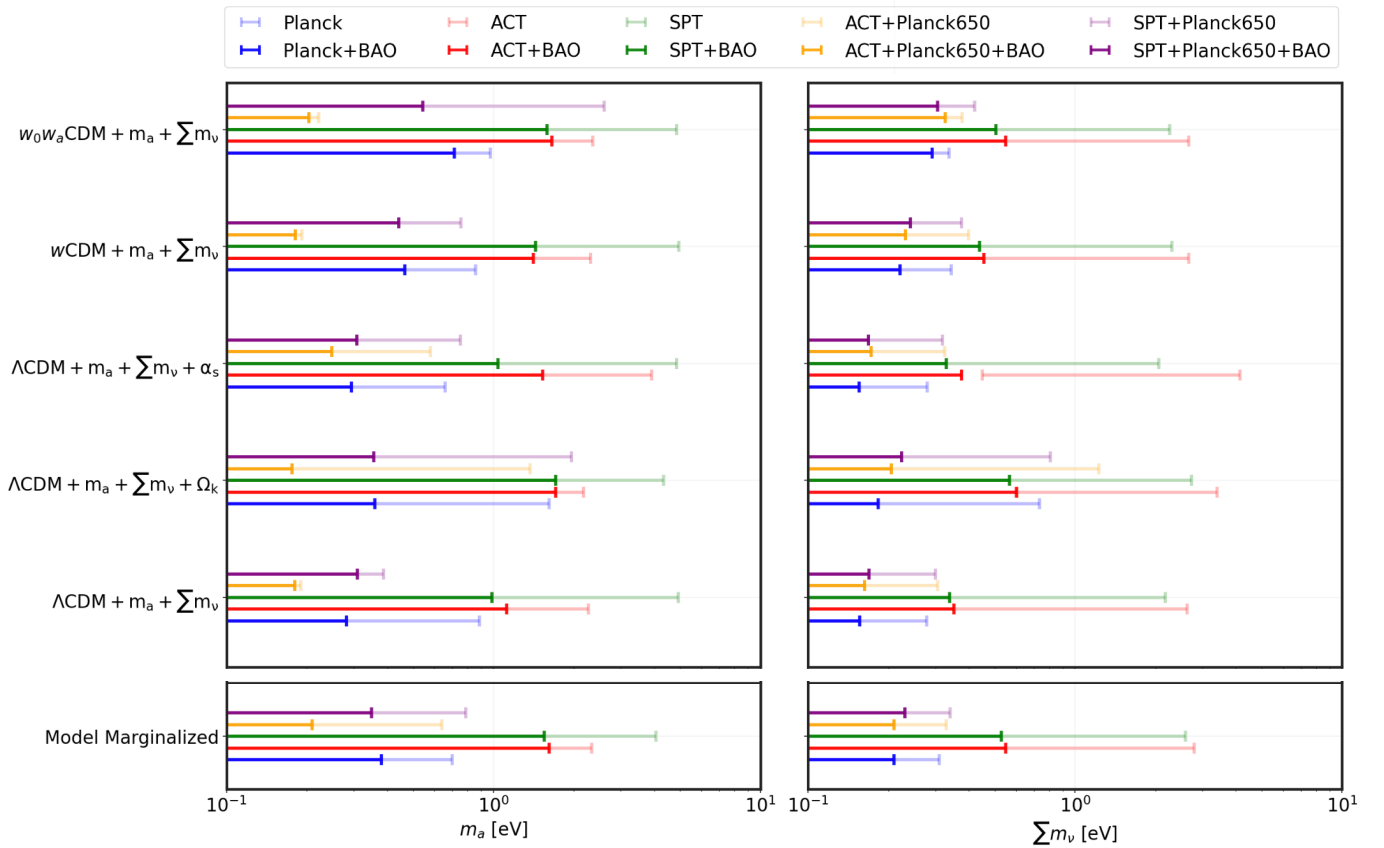


Figure 3: Whisker plot with the 95% CL upper bounds on the axion mass m_a (left) and on the total neutrino mass $\sum m_\nu$ (right) for different data combinations. The darker (lighter) lines depict the CMB limits with (without) the addition of BAO measurements. The top panels refer to constraints in each of the five possible background cosmologies explored here, while the lower panels show the model-marginalized ones derived here, see the main text of the manuscript for details.

equation of state: if w_0 is allowed to freely change including also the phantom region, Ω_m can take very high values and also the neutrino mass can be much higher than in standard cosmological backgrounds. Our next step is to consider the widely exploited, two-parameter CPL parameterization for the dark energy component, see Eq. (9). The results for this model are summarized in Appendix A, Table IX. The constraints in for w_0 are very similar to those previously described, preferring all CMB observations values of $w_0 < -1$ albeit with a mild significance. The corresponding H_0 value is also considerably larger than within the Λ CDM scenario (with hot relics). However, in this case, the addition of BAO data shifts the mean value of w_0 to the non-phantom region, with a very mild preference ($\sim 1.5\sigma$) for $w_0 > -1$. Notice that CMB data alone is unable to measure the time derivative of the dark energy equation of state w_a , providing only an upper bound on this parameter. When BAO information is also considered in the analyses, a mean value of $w_a \sim -1$ is preferred. The mean value of the Hubble constant after the inclusion of BAO observations is much closer to the value measured by the Planck collabora-

tion in a standard cosmology. The results above for the dark energy parameters are illustrated by means of the whisker plots for the w_0 and w_a parameters depicted in Figure 1. Concerning the hot relics, notice that this background cosmology, having two extra parameters largely degenerated with the neutrino masses, leads to the least constraining hot relic mass bounds: the most powerful combination sets 95% CL limits of $m_a < 0.20$ eV for the axion mass and $\sum m_\nu < 0.33$ eV for the total neutrino mass.

Table III presents the Bayes factors with respect to the best model for each of the five possible background cosmologies considered here and for the different data combinations. Interestingly, the best background cosmology is never found within the minimal Λ CDM plus two hot dark matter relics,⁶ regardless of the data set

⁶ It is important to note that, for all datasets, Λ CDM is favored over the baseline hot relic extension that is considered in this work. This result is consistent with previous studies, such as Ref.[71], which discussed similar findings with regards to the effects of relic neutrinos.

combinations. The combination of Planck or Planck650 with either BAO, SPT or ACT prefers a universe with a non-zero value of the running in the primordial power spectrum with strong evidence. Ground-based small-scale CMB probes, both alone and combined with BAO, prefer either non-flat universes, as in the case of SPT, or a model with a time varying dark energy component, as in the case of ACT. Such evidences are substantial when including BAO measurements.

Figure 2 shows the model-marginalized relative belief updating ratio \mathcal{R} , Eq. (8), for both the axion mass m_a (left) and for the sum of the neutrino masses $\sum m_\nu$ (right), considering the extensions of the Λ CDM model considered and using ACT + Planck650 + BAO (SPT + Planck650 + BAO) data. The horizontal lines show the significance levels $\exp(-1)$ and $\exp(-3)$. The vertical lines indicate the value 0.1 eV, corresponding to the approximate lower limits for $\sum m_\nu$ in the inverted ordering case. The quantity \mathcal{R} is independent of the shape and normalization of the prior and it is statistically equivalent to a Bayes factor between a model where m_a (m_ν) has been fixed to some value and another model where $m_a = 0$ ($m_\nu = 0$). The red curve shows the model-marginalized function \mathcal{R} , from which we derive the limits in Table IV. The black and gray lines show the \mathcal{R} function within each model, where the darker lines are those that contribute most to the model marginalization, that is, they have the best Bayesian evidences. For instance, for the case of ACT + Planck650 + BAO, the 95% CL marginalized limit is 0.21 eV, for both m_a and $\sum m_\nu$. Those bounds are led by the models which have the best Bayesian evidences, which, for this particular data combination, are the Λ CDM + m_a + $\sum m_\nu$ + Ω_k and the Λ CDM + m_a + $\sum m_\nu$ + α_s ones, see Table III, corresponding to the 95% CL upper bounds of $m_a < 0.176$ eV, $\sum m_\nu < 0.205$ eV and $m_a < 0.248$ eV, $\sum m_\nu < 0.172$ eV, respectively. Instead, for the other data combination illustrated in Figure 2, that is, SPT + Planck650 + BAO, the 95% CL marginalized limits are 0.35 eV and 0.23, for m_a and $\sum m_\nu$ respectively. Those bounds are led by the models which have the best Bayesian evidences, which, for this particular data combination, are the Λ CDM + m_a + $\sum m_\nu$ + α_s and the Λ CDM + m_a + $\sum m_\nu$ + Ω_k ones, see Table III, corresponding to the 95% CL upper bounds of $m_a < 0.308$ eV, $\sum m_\nu < 0.168$ eV and $m_a < 0.356$ eV, $\sum m_\nu < 0.224$ eV, respectively. Interestingly, the minimal Λ CDM cosmology never provides the best Bayesian evidence, for any of these two data combinations. Notice also that, while the ACT + Planck650 + BAO data combination provides more powerful limits on m_a than the SPT + Planck650 + BAO one, these two data sets are equally powerful when constraining the neutrino mass, as can be noticed from the results shown in Table IV.

We conclude this section by summarizing our results in the whisker plots shown in Figure 3, illustrating the 95% CL upper bounds on the axion mass m_a and on the total neutrino mass $\sum m_\nu$ arising for different data com-

binations in each of the five background cosmologies here. We also depict the model-marginalized limits on these two quantities. For the data combination Planck650 + ACT + BAO, the most constraining bound for m_a is obtained within the Λ CDM + m_a + $\sum m_\nu$ + Ω_k scenario ($m_a < 0.176$ eV at 95% CL). For the total neutrino mass, the tightest 95% CL upper bound ($m_a < 0.163$ eV at 95% CL) is found in the Λ CDM + m_a + $\sum m_\nu$ canonical scheme. For the data set SPT + Planck650 + BAO, the tightest limits on the hot thermal relic masses are those derived in the Λ CDM + m_a + $\sum m_\nu$ + α_s cosmological background, and correspond to $m_a < 0.301$ eV and $\sum m_\nu < 0.168$ eV (both at 95% CL).

IV. CONCLUSIONS

Axions provide the most elegant solution to the strong CP problem in Quantum Chromodynamics. In the early universe, axions can be produced via thermal or non thermal processes. Indeed, an axion population produced by scattering and decays of particles can provide additional radiation energy-density contributing to the hot dark matter component of the Universe, similarly to massive neutrinos. Therefore, it is certainly possible to set thermal axion mass limits from cosmology. Previous works in the literature have computed the current thermal axion population based on chiral perturbation theory. However, these limits can not be extended to high temperatures in the early universe because the underlying perturbation theory would not longer be valid. A possible method to overcome this problem makes use of an interpolation of the thermalization rate in order to cover the gap between the highest safe temperature reachable by chiral perturbation theory and the regime above the confinement scale, where the axion production rate is instead dominated by the axion-gluon scattering [39, 40].

Nevertheless, all previous axion mass bounds in the literature assume the minimal flat Λ CDM and neglect the other ground-based small-scale CMB measurements than those of *Planck* satellite observations.

Here we relax the two above assumptions and present novel model-marginalized limits on mixed hot dark matter scenarios, which consider both thermal neutrinos and thermal QCD axions. A new aspect of our analyses is the inclusion of small-scale Cosmic Microwave Background (CMB) observations from the Atacama Cosmology Telescope (ACT) and the South Pole Telescope (SPT), together with those from the Planck satellite and Baryon Acoustic Oscillation (BAO) data. The tightest 95% CL marginalised limits are 0.21 eV, for both $\sum m_\nu$ and m_a , from the combination of ACT, Planck650 and BAO measurements. Restricting the analyses to the standard Λ CDM picture extended with free neutrino and axion masses, we find $\sum m_\nu < 0.16$ eV and $m_a < 0.18$ eV, both at 95% CL. Interestingly, the best background cosmology is never found within the minimal Λ CDM plus hot relics, regardless of the data sets exploited in the analyses. The

Model	Planck		ACT		SPT		ACT+Planck650		SPT+Planck650	
	+BAO		+BAO		+BAO		+BAO		+BAO	
Λ CDM + m_a + $\sum m_\nu$	6.73	6.46	0.25	3.06	1.43	3.38	4.71	5.06	4.41	5.29
Λ CDM + m_a + $\sum m_\nu$ + α_s	0.00	0.00	6.35	4.39	0.22	0.79	0.00	0.45	0.00	0.00
Λ CDM + m_a + $\sum m_\nu$ + Ω_k	5.15	0.13	1.84	0.80	0.00	0.00	7.38	0.00	5.51	0.82
w ACDM + m_a + $\sum m_\nu$	5.50	1.64	0.26	0.78	2.75	1.66	5.37	2.37	5.55	1.82
$w_0 w_a$ ACDM + m_a + $\sum m_\nu$	5.35	1.62	0.00	0.00	2.36	0.70	5.68	2.37	7.29	1.51

Table III: Negative logarithms of the Bayes factors with respect to the best model for different data combinations, see also Appendix B.

Parameter	Planck		ACT		SPT		ACT+Planck650		SPT+Planck650	
	+BAO		+BAO		+BAO		+BAO		+BAO	
m_a [eV] (68 %)	< 0.18	< 0.14	< 1.01	< 0.71	< 2.15	< 0.69	< 0.13	< 0.09	< 0.20	< 0.14
m_a [eV] (95 %)	< 0.70	< 0.38	< 2.33	< 1.62	< 4.06	< 1.55	< 0.64	< 0.21	< 0.79	< 0.35
$\sum m_\nu$ [eV] (68 %)	< 0.16	< 0.12	< 1.42	< 0.29	< 1.29	< 0.29	< 0.16	< 0.12	< 0.17	< 0.13
$\sum m_\nu$ [eV] (95 %)	< 0.31	< 0.21	< 2.79	< 0.55	< 2.59	< 0.53	< 0.33	< 0.21	< 0.34	< 0.23

Table IV: Marginalized upper bounds on m_a and $\sum m_\nu$ in eV for different data combinations.

combination of Planck or Planck 650 with either BAO, SPT or ACT prefers a universe with a non-zero value of the running in the primordial power spectrum with strong evidence. Ground-based small-scale CMB probes, both alone and combined with BAO, prefer either with substantial evidence for non-flat universes, as in the case of SPT, or a model with a time varying dark energy component, as in the case of ACT. If the existence of an axion which may be thermally produced in the early universe and neutrino masses will be independently confirmed by other probes, upcoming cosmological observations may strengthen the evidence against the minimal cosmological framework, pointing to possible exciting new ingredients in the theory.

ACKNOWLEDGMENTS

EDV is supported by a Royal Society Dorothy Hodgkin Research Fellowship. This article is based upon work from COST Action CA21136 Addressing observational tensions in cosmology with systematics and fundamental physics (CosmoVerse) supported by COST (European Cooperation in Science and Technology). AM and WG are supported by the TASP INFN initiative. We

acknowledge IT Services at The University of Sheffield for the provision of services for High Performance Computing. This work has been partially supported by the MCIN/AEI/10.13039/501100011033 of Spain under grant PID2020-113644GB-I00, by the Generalitat Valenciana of Spain under grant PROMETEO/2019/083 and by the European Union's Framework Programme for Research and Innovation Horizon 2020 (2014–2020) under grant agreement 754496 (FELLINI) and 860881 (HID-DeN).

DATA AVAILABILITY

The data and chains underlying this article will be shared on reasonable request to the corresponding author.

Appendix A: Tables

In this appendix we provide the tables with all the results for the cosmological parameters for all the models discussed in our work:

Cosmological Model	Results in
$\Lambda\text{CDM}+\sum m_\nu+m_a$	Table V
$\Lambda\text{CDM}+\sum m_\nu+m_a+\Omega_k$	Table VI
$\Lambda\text{CDM}+\sum m_\nu+m_a+\alpha_s$	Table VII
$w\text{CDM}+\sum m_\nu+m_a$	Table VIII
$w_0w_a\text{CDM}+\sum m_\nu+m_a$	Table IX

Appendix B: Bayesian evidences and Bayes factors

In this appendix we provide a figure ([Figure 4](#)) reporting the Bayesian evidences for each model and within each dataset combination, and a figure ([Figure 5](#)) representing the Bayes factors listed in [table III](#).

Parameter	Planck		ACT		SPT		ACT+Planck650		SPT+Planck650	
	+BAO		+BAO		+BAO		+BAO		+BAO	
$\Omega_b h^2$	0.02243 ± 0.00015	0.02250 ± 0.00015	0.02165 ± 0.00033	0.02170 ± 0.00032	0.02251 ± 0.00033	0.02252 ± 0.00032	0.02238 ± 0.00014	0.02245 ± 0.00013	0.02246 ± 0.00014	0.02252 ± 0.00013
$\Omega_c h^2$	0.1225 ^{+0.0016} _{-0.0022}	0.1208 ^{+0.0012} _{-0.0014}	0.1242 ± 0.0046	0.1190 ^{+0.0024} _{-0.0020}	0.1195 ^{+0.0060} _{-0.0046}	0.1175 ^{+0.0022} _{-0.0020}	0.1214 ± 0.0015	0.1204 ^{+0.0011} _{-0.0012}	0.1216 ^{+0.0014} _{-0.0018}	0.1204 ^{+0.0012} _{-0.0014}
τ	0.0564 ± 0.0076	0.0581 ^{+0.0070} _{-0.0080}	0.072 ± 0.015	0.070 ± 0.015	0.067 ± 0.015	0.069 ± 0.014	0.0562 ^{+0.0072} _{-0.0082}	0.0567 ^{+0.0070} _{-0.0081}	0.0548 ± 0.0081	0.0556 ± 0.0078
100 θ_{MC}	1.04058 ± 0.00036	1.04081 ± 0.00032	1.04120 ± 0.00081	1.04208 ± 0.00064	1.03854 ± 0.00082	1.03939 ± 0.00066	1.04087 ± 0.00031	1.04101 ± 0.00027	1.04044 ± 0.00032	1.04060 ± 0.00029
n_s	0.9681 ± 0.0049	0.9703 ± 0.0043	1.005 ^{+0.022} _{-0.018}	1.022 ± 0.015	0.987 ^{+0.031} _{-0.024}	1.013 ± 0.018	0.9705 ± 0.0043	0.9727 ^{+0.0037} _{-0.0041}	0.9700 ± 0.0048	0.9721 ± 0.0043
$\log(10^{10} A_s)$	3.055 ^{+0.015} _{-0.016}	3.055 ^{+0.014} _{-0.016}	3.077 ± 0.032	3.063 ± 0.031	3.047 ± 0.035	3.035 ± 0.033	3.059 ± 0.016	3.057 ^{+0.014} _{-0.016}	3.047 ± 0.017	3.047 ± 0.016
m_a [eV]	< 0.888	< 0.282	< 2.27	< 1.12	< 4.93	< 0.987	< 0.190	< 0.180	< 0.388	< 0.310
$\sum m_\nu$ [eV]	< 0.278	< 0.156	< 2.63	< 0.351	< 2.18	< 0.339	< 0.305	< 0.163	< 0.300	< 0.169
H_0	66.9 ^{+1.2} _{-0.73}	67.90 ± 0.53	60 ⁺⁷ ₋₄	67.97 ± 0.77	61.1 ^{+6.3} _{-3.9}	68.50 ± 0.74	67.0 ^{+1.1} _{-0.73}	67.81 ± 0.52	67.1 ^{+1.1} _{-0.72}	67.95 ± 0.54
σ_8	0.793 ^{+0.023} _{-0.011}	0.8052 ^{+0.0099} _{-0.0075}	0.656 ^{+0.11} _{-0.076}	0.779 ^{+0.032} _{-0.026}	0.611 ^{+0.10} _{-0.081}	0.755 ^{+0.031} _{-0.024}	0.801 ^{+0.020} _{-0.011}	0.809 ^{+0.011} _{-0.0084}	0.791 ^{+0.020} _{-0.011}	0.799 ^{+0.012} _{-0.0087}

Table V: 95% CL upper bounds on the QCD axion mass and on the sum of neutrino masses and 68% CL cosmological parameter errors in the minimal Λ CDM picture.

Parameter	Planck		ACT		SPT		ACT+Planck650		SPT+Planck650	
	+BAO		+BAO		+BAO		+BAO		+BAO	
$\Omega_b h^2$	0.02256 ± 0.00020	0.02248 ± 0.00016	0.02178 ± 0.00033	0.02166 ± 0.00032	0.02253 ± 0.00034	0.02244 ± 0.00033	0.02249 ^{+0.00017} _{-0.00021}	0.02242 ± 0.00013	0.02261 ± 0.00018	0.02248 ± 0.00015
$\Omega_c h^2$	0.1214 ± 0.0020	0.1214 ^{+0.0016} _{-0.0019}	0.1182 ± 0.0047	0.1237 ± 0.0048	0.1163 ± 0.0063	0.1232 ± 0.0052	0.1203 ± 0.0016	0.1209 ± 0.0014	0.1210 ± 0.0019	0.1211 ^{+0.0015} _{-0.0018}
τ	0.0497 ± 0.0077	0.0589 ± 0.0070	0.065 ± 0.015	0.071 ± 0.014	0.065 ± 0.015	0.068 ± 0.015	0.0475 ± 0.0079	0.0566 ± 0.0077	0.0488 ± 0.0083	0.0552 ± 0.0079
100 θ_{MC}	1.04058 ± 0.00037	1.04072 ± 0.00034	1.04131 ± 0.00077	1.04157 ± 0.00075	1.03868 ± 0.00085	1.03886 ± 0.00081	1.04075 ± 0.00033	1.04094 ± 0.00029	1.04037 ± 0.00035	1.04052 ± 0.00032
n_s	0.9727 ± 0.0055	0.9697 ± 0.0049	1.004 ± 0.020	1.014 ± 0.017	0.994 ± 0.030	0.999 ± 0.022	0.9727 ± 0.0058	0.9716 ± 0.0043	0.9738 ± 0.0056	0.9709 ± 0.0049
$\log(10^{10} A_s)$	3.037 ± 0.017	3.058 ± 0.014	3.046 ± 0.033	3.075 ± 0.032	3.032 ± 0.039	3.049 ± 0.036	3.036 ± 0.017	3.058 ± 0.016	3.034 ± 0.018	3.047 ± 0.016
Ω_k	-0.029 ^{+0.016} _{-0.011}	0.0010 ± 0.0021	-0.169 ^{+0.070} _{-0.091}	0.0069 ^{+0.0057} _{-0.0065}	-0.057 ^{+0.075} _{-0.035}	0.0079 ^{+0.0060} _{-0.0068}	-0.091 ^{+0.047} _{-0.032}	0.0011 ± 0.0020	-0.047 ^{+0.029} _{-0.017}	0.0014 ^{+0.0019} _{-0.0022}
m_a [eV]	< 1.62	< 0.359	< 2.18	< 1.71	< 4.34	< 1.71	< 1.37	< 0.176	< 1.96	< 0.356
$\sum m_\nu$ [eV]	< 0.736	< 0.183	2.0 ^{+1.4} _{-1.4}	< 0.604	< 2.73	< 0.567	< 1.23	< 0.205	< 0.808	< 0.224
H_0	56.3 ± 4.3	68.14 ± 0.73	35.8 ^{+3.3} _{-2.6}	68.45 ± 0.94	50 ⁺⁹ ₋₁₀	69.07 ± 0.91	45.0 ^{+4.6} _{-2.6}	68.02 ± 0.69	52.7 ± 5.4	68.25 ± 0.73
σ_8	0.701 ± 0.047	0.805 ^{+0.011} _{-0.0085}	0.459 ^{+0.037} _{-0.069}	0.768 ^{+0.035} _{-0.030}	0.535 ^{+0.084} _{-0.12}	0.745 ^{+0.034} _{-0.030}	0.627 ^{+0.051} _{-0.077}	0.808 ^{+0.013} _{-0.0094}	0.688 ^{+0.067} _{-0.053}	0.797 ^{+0.015} _{-0.0098}

Table VI: 95% CL upper bounds on the QCD axion mass and on the sum of neutrino masses and 68% CL cosmological parameter errors in the presence of a non-zero curvature component.

Parameter	Planck		ACT		SPT		ACT+Planck650		SPT+Planck650	
	+BAO		+BAO		+BAO		+BAO		+BAO	
$\Omega_b h^2$	0.02245 ± 0.00016	0.02252 ± 0.00015	0.02137 ± 0.00033	0.02152 ± 0.00032	0.02249 ± 0.00034	0.02251 ± 0.00032	0.02234 ± 0.00014	0.02239 ± 0.00014	0.02247 ± 0.00015	0.02252 ± 0.00014
$\Omega_c h^2$	0.1223 ^{+0.0016} _{-0.0021}	0.1208 ^{+0.0011} _{-0.0014}	0.1240 ^{+0.0051} _{-0.0045}	0.1185 ^{+0.0024} _{-0.0021}	0.1186 ^{+0.0060} _{-0.0047}	0.1174 ^{+0.0023} _{-0.0019}	0.1217 ^{+0.0014} _{-0.0018}	0.1205 ^{+0.0011} _{-0.0014}	0.1218 ^{+0.0017} _{-0.0020}	0.1204 ^{+0.0012} _{-0.0014}
τ	0.0572 ^{+0.0073} _{-0.0082}	0.0598 ± 0.0070	0.064 ± 0.015	0.066 ± 0.015	0.066 ± 0.015	0.066 ± 0.014	0.0543 ± 0.0078	0.0551 ± 0.0077	0.0549 ± 0.0079	0.0556 ± 0.0080
100 θ_{MC}	1.04061 ± 0.00035	1.04082 ± 0.00031	1.04079 ± 0.00075	1.04222 ± 0.00064	1.03864 ± 0.00084	1.03943 ± 0.00065	1.04083 ± 0.00032	1.04098 ± 0.00028	1.04041 ± 0.00033	1.04060 ± 0.00028
n_s	0.9677 ± 0.0052	0.9700 ± 0.0045	0.916 ^{+0.024} _{-0.027}	0.986 ± 0.019	0.969 ± 0.034	1.001 ^{+0.025} _{-0.029}	0.9724 ^{+0.0044} _{-0.0050}	0.9740 ^{+0.0040} _{-0.0046}	0.9703 ± 0.0052	0.9722 ± 0.0046
$\log(10^{10} A_s)$	3.057 ± 0.016	3.058 ± 0.015	3.068 ± 0.031	3.055 ± 0.030	3.041 ± 0.035	3.029 ± 0.034	3.053 ± 0.017	3.051 ± 0.016	3.048 ± 0.017	3.046 ± 0.017
α_s	-0.0027 ± 0.0071	-0.0029 ± 0.0067	0.133 ± 0.028	0.086 ± 0.029	0.048 ± 0.054	0.031 ± 0.054	0.0083 ± 0.0064	0.0080 ± 0.0063	0.0004 ± 0.0068	0.0003 ± 0.0067
m_a [eV]	< 0.661	< 0.294	< 3.92	< 1.53	< 4.86	< 1.04	< 0.580	< 0.248	< 0.753	< 0.308
$\sum m_\nu$ [eV]	< 0.279	< 0.155	2.3 ^{+1.9} _{-1.8}	< 0.375	< 2.06	< 0.329	< 0.325	< 0.172	< 0.318	< 0.168
H_0	67.0 ^{+1.1} _{-0.76}	67.93 ± 0.52	51.0 ^{+3.5} _{-2.2}	68.00 ^{+0.74} _{-0.66}	61.0 ^{+5.8} _{-4.1}	68.54 ± 0.72	66.9 ^{+1.2} _{-0.72}	67.79 ± 0.53	67.0 ^{+1.2} _{-0.77}	67.96 ± 0.54
σ_8	0.794 ^{+0.021} _{-0.010}	0.8057 ^{+0.0098} _{-0.0072}	0.489 ^{+0.045} _{-0.073}	0.756 ± 0.031	0.600 ^{+0.097} _{-0.083}	0.753 ^{+0.031} _{-0.026}	0.795 ^{+0.026} _{-0.012}	0.807 ^{+0.012} _{-0.0086}	0.786 ^{+0.027} _{-0.013}	0.799 ^{+0.012} _{-0.0088}

Table VII: 95% CL upper bounds on the QCD axion mass and on the sum of neutrino masses and 68% CL cosmological parameter errors in the presence of a running of the scalar tilt in the primordial power spectrum.

Parameter	Planck		ACT		SPT		ACT+Planck650		SPT+Planck650	
	+BAO		+BAO		+BAO		+BAO		+BAO	
$\Omega_b h^2$	0.02247 ± 0.00017	0.02248 ± 0.00015	0.02166 ± 0.00032	0.02169 ± 0.00032	0.02249 ± 0.00033	0.02252 ± 0.00033	0.02241 ± 0.00014	0.02242 ± 0.00013	0.02249 ± 0.00015	0.02251 ± 0.00014
$\Omega_c h^2$	0.1221 ^{+0.0018} _{-0.0023}	0.1215 ^{+0.0013} _{-0.0018}	0.1243 ± 0.0045	0.1191 ± 0.0026	0.1198 ^{+0.0062} _{-0.0048}	0.1179 ± 0.0025	0.1212 ± 0.0015	0.1208 ± 0.0013	0.1216 ^{+0.0016} _{-0.0020}	0.1210 ^{+0.0014} _{-0.0017}
τ	0.0547 ± 0.0077	0.0566 ± 0.0077	0.072 ± 0.015	0.070 ± 0.015	0.067 ± 0.015	0.068 ± 0.014	0.0556 ± 0.0079	0.0559 ^{+0.0073} _{-0.0081}	0.0542 ± 0.0075	0.0548 ± 0.0078
100 θ_{MC}	1.04060 ± 0.00037	1.04071 ± 0.00032	1.04114 ± 0.00080	1.04201 ± 0.00068	1.03846 ± 0.00083	1.03932 ± 0.00068	1.04088 ± 0.00030	1.04096 ± 0.00029	1.04043 ± 0.00034	1.04052 ± 0.00031
n_s	0.9695 ± 0.0050	0.9697 ± 0.0046	1.003 ^{+0.022} _{-0.019}	1.023 ± 0.015	0.983 ^{+0.029} _{-0.026}	1.013 ± 0.018	0.9708 ± 0.0044	0.9718 ± 0.0041	0.9705 ± 0.0049	0.9716 ± 0.0046
$\log(10^{10} A_s)$	3.050 ± 0.016	3.053 ± 0.015	3.078 ± 0.033	3.062 ± 0.031	3.049 ± 0.036	3.034 ± 0.034	3.056 ± 0.016	3.056 ± 0.016	3.046 ± 0.016	3.046 ± 0.016
w_0	-1.64 ^{+0.22} _{-0.33}	-1.052 ^{+0.061} _{-0.047}	-1.70 ± 0.63	-1.035 ^{+0.098} _{-0.074}	-1.55 ^{+0.80} _{-0.67}	-1.051 ^{+0.098} _{-0.075}	-1.62 ^{+0.24} _{-0.34}	-1.039 ^{+0.057} _{-0.046}	-1.58 ^{+0.25} _{-0.36}	-1.044 ^{+0.062} _{-0.047}
m_a [eV]	< 0.858	< 0.466	< 2.31	< 1.41	< 4.96	< 1.44	< 0.192	< 0.181	< 0.755	< 0.442
$\sum m_\nu$ [eV]	< 0.343	< 0.221	< 2.67	< 0.455	< 2.30	< 0.438	< 0.400	< 0.232	< 0.376	< 0.242
H_0	> 83.1	69.0 ^{+1.2} _{-1.4}	72 ⁺¹⁰ ₋₂₀	68.5 ^{+1.6} _{-1.8}	71 ⁺¹⁰ ₋₂₀	69.4 ^{+1.6} _{-1.9}	> 82.1	68.6 ^{+1.1} _{-1.3}	> 80.5	68.9 ^{+1.2} _{-1.4}
σ_8	0.945 ^{+0.083} _{-0.053}	0.812 ± 0.014	0.73 ± 0.14	0.775 ^{+0.031} _{-0.028}	0.66 ^{+0.12} _{-0.14}	0.751 ^{+0.031} _{-0.028}	0.955 ^{+0.090} _{-0.057}	0.815 ± 0.015	0.926 ^{+0.092} _{-0.062}	0.804 ± 0.016

Table VIII: 95% CL upper bounds on the QCD axion mass and on the sum of neutrino masses and 68% CL cosmological parameter errors varying the dark energy equation of state.

Parameter	Planck		ACT		SPT		ACT+Planck650		SPT+Planck650	
	+BAO		+BAO		+BAO		+BAO		+BAO	
$\Omega_b h^2$	0.02248 ± 0.00017	0.02245 ± 0.00015	0.02166 ± 0.00033	0.02168 ± 0.00032	0.02249 ± 0.00033	0.02249 ± 0.00033	0.02241 ± 0.00014	0.02239 ± 0.00013	0.02252 ± 0.00016	0.02247 ± 0.00014
$\Omega_c h^2$	0.1220 ^{+0.0018} _{-0.0022}	0.1223 ^{+0.0015} _{-0.0020}	0.1241 ± 0.0045	0.1207 ± 0.0029	0.1198 ^{+0.0059} _{-0.0046}	0.1191 ± 0.0028	0.1212 ^{+0.0014} _{-0.0016}	0.1214 ^{+0.0012} _{-0.0014}	0.1217 ^{+0.0018} _{-0.0022}	0.1216 ^{+0.0015} _{-0.0018}
τ	0.0547 ± 0.0076	0.0557 ^{+0.0071} _{-0.0082}	0.072 ± 0.015	0.070 ± 0.015	0.067 ± 0.015	0.067 ± 0.015	0.0554 ± 0.0077	0.0556 ± 0.0079	0.0542 ± 0.0078	0.0545 ^{+0.0070} _{-0.0078}
100 θ_{MC}	1.04062 ± 0.00037	1.04060 ± 0.00034	1.04117 ± 0.00081	1.04185 ± 0.00068	1.03846 ± 0.00080	1.03921 ± 0.00070	1.04088 ± 0.00031	1.04087 ± 0.00029	1.04035 ± 0.00035	1.04044 ± 0.00031
n_s	0.9697 ± 0.0051	0.9691 ± 0.0047	1.004 ^{+0.022} _{-0.019}	1.021 ± 0.015	0.984 ^{+0.029} _{-0.025}	1.010 ± 0.019	0.9711 ± 0.0045	0.9707 ± 0.0042	0.9702 ^{+0.0058} _{-0.0052}	0.9705 ± 0.0047
$\log(10^{10} A_s)$	3.050 ± 0.016	3.053 ^{+0.015} _{-0.017}	3.076 ± 0.032	3.066 ± 0.031	3.048 ± 0.036	3.035 ± 0.034	3.056 ± 0.016	3.057 ± 0.016	3.048 ± 0.017	3.047 ^{+0.015} _{-0.016}
w_0	-1.32 ^{+0.43} _{-0.55}	-0.70 ± 0.21	-1.46 ^{+0.72} _{-1.1}	-0.80 ± 0.25	-1.30 ^{+0.83} _{-1.1}	-0.88 ± 0.24	-1.30 ^{+0.44} _{-0.58}	-0.70 ± 0.22	-1.10 ^{+0.47} _{-0.70}	-0.74 ± 0.22
w_a	< -0.693	-1.14 ^{+0.79} _{-0.65}	< -0.325	-0.96 ^{+1.0} _{-0.85}	< -0.284	-0.70 ^{+1.0} _{-0.74}	< -0.671	-1.10 ^{+0.80} _{-0.64}	< -1.19	-0.99 ^{+0.80} _{-0.63}
m_a [eV]	< 0.972	< 0.716	< 2.36	< 1.66	< 4.85	< 1.59	< 0.222	< 0.204	< 2.60	< 0.544
$\sum m_\nu$ [eV]	< 0.337	< 0.291	< 2.66	< 0.549	< 2.26	< 0.505	< 0.378	< 0.326	< 0.420	< 0.305
H_0	> 80.4	66.7 ^{+1.7} _{-2.0}	71 ⁺¹⁰ ₋₂₀	67.3 ^{+1.9} _{-2.3}	70 ⁺¹⁰ ₋₂₀	68.4 ^{+2.1} _{-2.3}	> 79.6	66.2 ± 1.9	> 75.3	66.8 ± 1.9
σ_8	0.929 ^{+0.10} _{-0.060}	0.791 ± 0.019	0.72 ± 0.14	0.766 ^{+0.034} _{-0.030}	0.65 ^{+0.12} _{-0.14}	0.745 ± 0.031	0.941 ^{+0.11} _{-0.063}	0.796 ± 0.020	0.880 ^{+0.14} _{-0.070}	0.789 ± 0.020

Table IX: 95% CL upper bounds on the QCD axion mass and on the sum of neutrino masses and 68% CL cosmological parameter errors varying the dark energy equation of state using the CPL two-parameter parameterization, see Eq. (9).

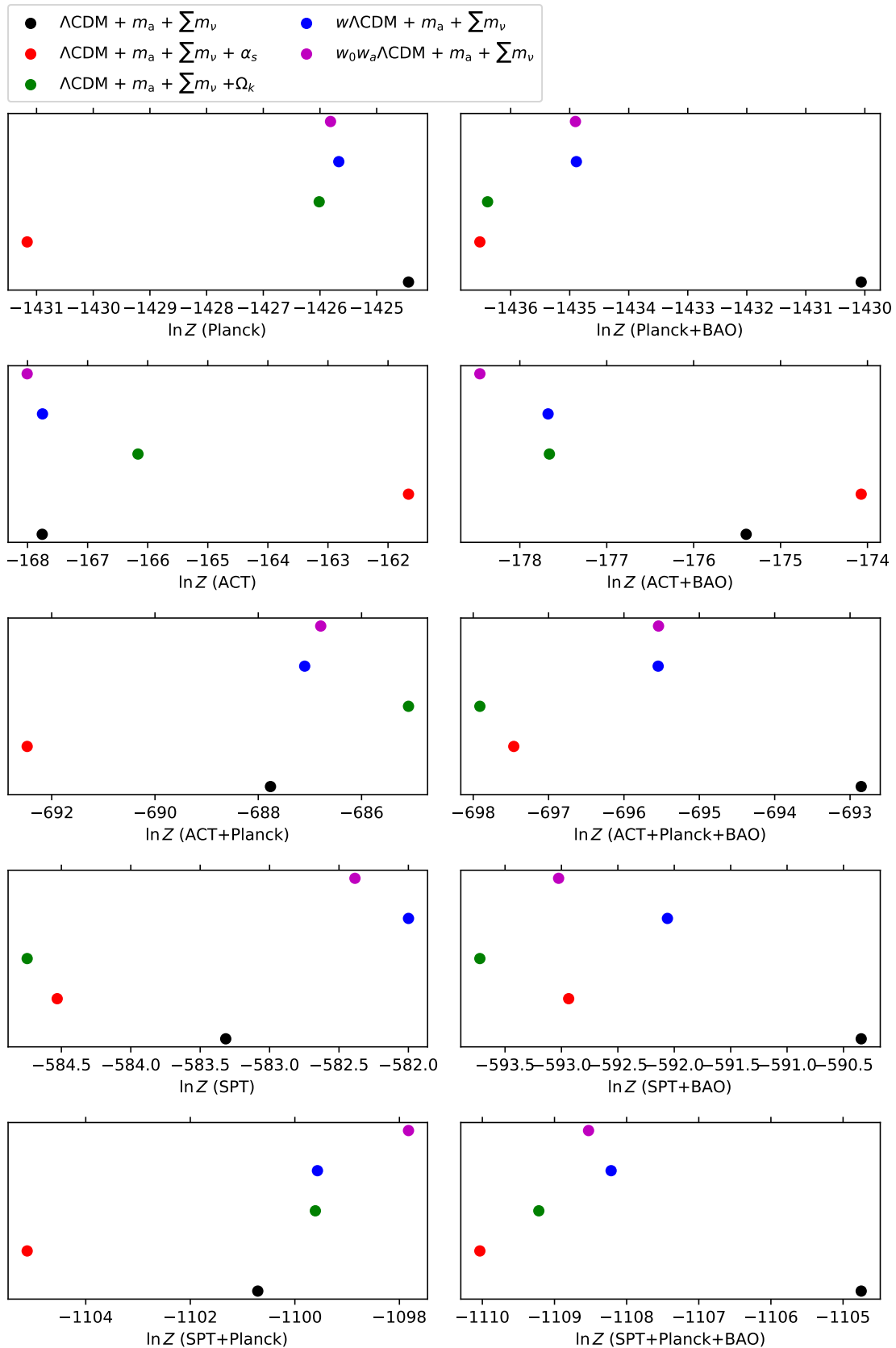


Figure 4: Bayesian evidences for each model and dataset combination.

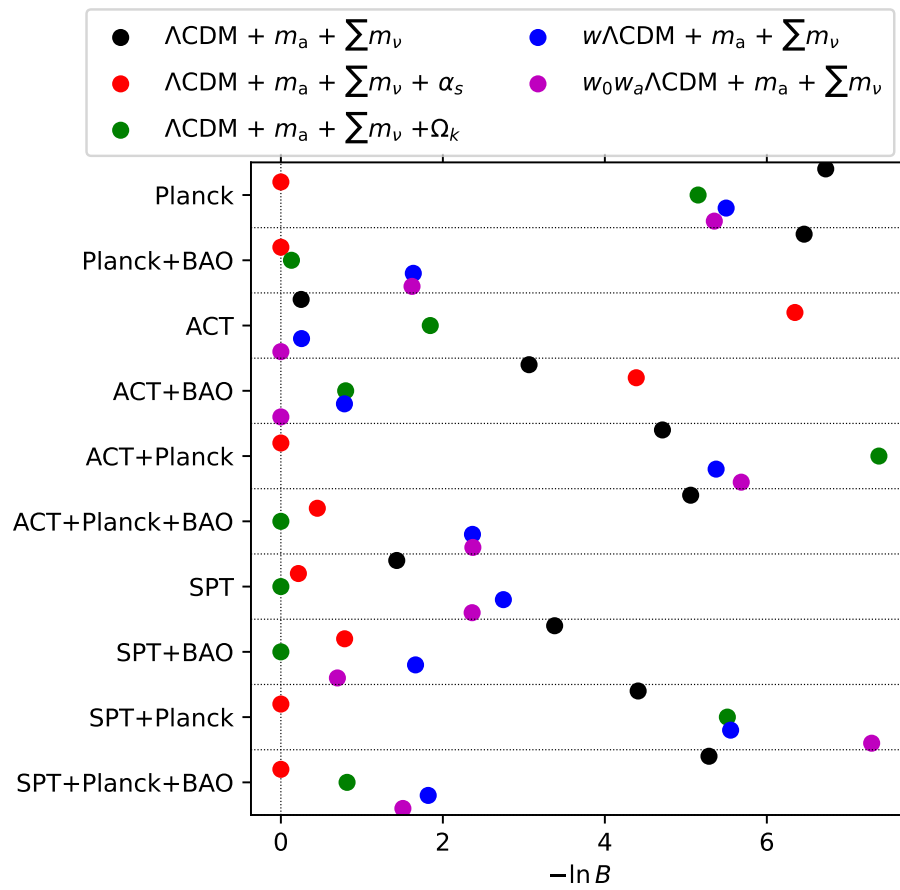


Figure 5: Bayes factors, normalized to the best model for each dataset.

-
- [1] R. D. Peccei and H. R. Quinn, *Phys. Rev. Lett.* **38**, 1440 (1977).
- [2] R. D. Peccei and H. R. Quinn, *Phys. Rev. D* **16**, 1791 (1977).
- [3] C. A. Baker *et al.*, *Phys. Rev. Lett.* **97**, 131801 (2006), [arXiv:hep-ex/0602020](#).
- [4] J. M. Pendlebury *et al.*, *Phys. Rev. D* **92**, 092003 (2015), [arXiv:1509.04411 \[hep-ex\]](#).
- [5] C. Abel *et al.*, *Phys. Rev. Lett.* **124**, 081803 (2020), [arXiv:2001.11966 \[hep-ex\]](#).
- [6] F. Wilczek, *Phys. Rev. Lett.* **40**, 279 (1978).
- [7] S. Weinberg, *Phys. Rev. Lett.* **40**, 223 (1978).
- [8] C. Vafa and E. Witten, *Phys. Rev. Lett.* **53**, 535 (1984).
- [9] L. Di Luzio, M. Giannotti, E. Nardi, and L. Visinelli, *Phys. Rept.* **870**, 1 (2020), [arXiv:2003.01100 \[hep-ph\]](#).
- [10] L. F. Abbott and P. Sikivie, *Phys. Lett. B* **120**, 133 (1983).
- [11] M. Dine and W. Fischler, *Phys. Lett. B* **120**, 137 (1983).
- [12] J. Preskill, M. B. Wise, and F. Wilczek, *Phys. Lett. B* **120**, 127 (1983).
- [13] A. D. Linde, *Phys. Lett. B* **158**, 375 (1985).
- [14] D. Seckel and M. S. Turner, *Phys. Rev. D* **32**, 3178 (1985).
- [15] D. H. Lyth, *Phys. Lett. B* **236**, 408 (1990).
- [16] A. D. Linde and D. H. Lyth, *Phys. Lett. B* **246**, 353 (1990).
- [17] A. Vilenkin and E. P. S. Shellard, *Cosmic Strings and Other Topological Defects* (Cambridge University Press, 2000).
- [18] T. W. B. Kibble, *J. Phys. A* **9**, 1387 (1976).
- [19] T. W. B. Kibble, G. Lazarides, and Q. Shafi, *Phys. Rev. D* **26**, 435 (1982).
- [20] A. Vilenkin, *Phys. Rev. D* **24**, 2082 (1981).
- [21] R. L. Davis, *Phys. Lett. B* **180**, 225 (1986).
- [22] A. Vilenkin and A. E. Everett, *Phys. Rev. Lett.* **48**, 1867 (1982).
- [23] P. Sikivie, *Phys. Rev. Lett.* **48**, 1156 (1982).
- [24] M. C. Huang and P. Sikivie, *Phys. Rev. D* **32**, 1560 (1985).
- [25] S. Hannestad, A. Mirizzi, and G. Raffelt, *JCAP* **07**, 002 (2005), [arXiv:hep-ph/0504059](#).
- [26] A. Melchiorri, O. Mena, and A. Slosar, *Phys. Rev. D* **76**, 041303 (2007), [arXiv:0705.2695 \[astro-ph\]](#).
- [27] S. Hannestad, A. Mirizzi, G. G. Raffelt, and Y. Y. Y. Wong, *JCAP* **08**, 015 (2007), [arXiv:0706.4198 \[astro-ph\]](#).
- [28] S. Hannestad, A. Mirizzi, G. G. Raffelt, and Y. Y. Y. Wong, *JCAP* **04**, 019 (2008), [arXiv:0803.1585 \[astro-ph\]](#).
- [29] S. Hannestad, A. Mirizzi, G. G. Raffelt, and Y. Y. Y. Wong, *JCAP* **08**, 001 (2010), [arXiv:1004.0695 \[astro-ph.CO\]](#).
- [30] M. Archidiacono, S. Hannestad, A. Mirizzi, G. Raffelt, and Y. Y. Y. Wong, *JCAP* **10**, 020 (2013), [arXiv:1307.0615 \[astro-ph.CO\]](#).
- [31] E. Giusarma, E. Di Valentino, M. Lattanzi, A. Melchiorri, and O. Mena, *Phys. Rev. D* **90**, 043507 (2014), [arXiv:1403.4852 \[astro-ph.CO\]](#).
- [32] E. Di Valentino, S. Gariazzo, E. Giusarma, and O. Mena, *Phys. Rev. D* **91**, 123505 (2015), [arXiv:1503.00911 \[astro-ph.CO\]](#).
- [33] E. Di Valentino, E. Giusarma, M. Lattanzi, O. Mena, A. Melchiorri, and J. Silk, *Phys. Lett. B* **752**, 182 (2016), [arXiv:1507.08665 \[astro-ph.CO\]](#).
- [34] M. Archidiacono, T. Basse, J. Hamann, S. Hannestad, G. Raffelt, and Y. Y. Y. Wong, *JCAP* **05**, 050 (2015), [arXiv:1502.03325 \[astro-ph.CO\]](#).
- [35] R. Z. Ferreira, A. Notari, and F. Rompineve, *Phys. Rev. D* **103**, 063524 (2021), [arXiv:2012.06566 \[hep-ph\]](#).
- [36] L. Di Luzio, G. Martinelli, and G. Piazza, *Phys. Rev. Lett.* **126**, 241801 (2021), [arXiv:2101.10330 \[hep-ph\]](#).
- [37] W. Giarè, E. Di Valentino, A. Melchiorri, and O. Mena, *Mon. Not. Roy. Astron. Soc.* **505**, 2703 (2021), [arXiv:2011.14704 \[astro-ph.CO\]](#).
- [38] L. Di Luzio and G. Piazza, (2022), [arXiv:2206.04061 \[hep-ph\]](#).
- [39] F. D’Eramo, F. Hajkarim, and S. Yun, *Phys. Rev. Lett.* **128**, 152001 (2022), [arXiv:2108.04259 \[hep-ph\]](#).
- [40] F. D’Eramo, F. Hajkarim, and S. Yun, *JHEP* **10**, 224 (2021), [arXiv:2108.05371 \[hep-ph\]](#).
- [41] F. D’Eramo, E. Di Valentino, W. Giarè, F. Hajkarim, A. Melchiorri, O. Mena, F. Renzi, and S. Yun, *JCAP* **09**, 022 (2022), [arXiv:2205.07849 \[astro-ph.CO\]](#).
- [42] J. E. Kim, *Phys. Rev. Lett.* **43**, 103 (1979).
- [43] M. A. Shifman, A. I. Vainshtein, and V. I. Zakharov, *Nucl. Phys. B* **166**, 493 (1980).
- [44] M. Dine, W. Fischler, and M. Srednicki, *Phys. Lett. B* **104**, 199 (1981).
- [45] A. R. Zhitnitsky, *Sov. J. Nucl. Phys.* **31**, 260 (1980).
- [46] L. Caloni, M. Gerbino, M. Lattanzi, and L. Visinelli, *JCAP* **09**, 021 (2022), [arXiv:2205.01637 \[astro-ph.CO\]](#).
- [47] L. Di Luzio, F. Mescia, and E. Nardi, *Phys. Rev. Lett.* **118**, 031801 (2017), [arXiv:1610.07593 \[hep-ph\]](#).
- [48] L. Di Luzio, F. Mescia, and E. Nardi, *Phys. Rev. D* **96**, 075003 (2017), [arXiv:1705.05370 \[hep-ph\]](#).
- [49] V. Plakkot and S. Hoof, *Phys. Rev. D* **104**, 075017 (2021), [arXiv:2107.12378 \[hep-ph\]](#).
- [50] J. Diehl and E. Koutsangelas, (2023), [arXiv:2302.04667 \[hep-ph\]](#).
- [51] N. Aghanim *et al.* (Planck), *Astron. Astrophys.* **641**, A5 (2020), [arXiv:1907.12875 \[astro-ph.CO\]](#).
- [52] N. Aghanim *et al.* (Planck), *Astron. Astrophys.* **641**, A6 (2020), [arXiv:1807.06209 \[astro-ph.CO\]](#).
- [53] N. Aghanim *et al.* (Planck), *Astron. Astrophys.* **641**, A1 (2020), [arXiv:1807.06205 \[astro-ph.CO\]](#).
- [54] N. Aghanim *et al.* (Planck), *Astron. Astrophys.* **641**, A8 (2020), [arXiv:1807.06210 \[astro-ph.CO\]](#).
- [55] E. Aver, K. A. Olive, and E. D. Skillman, *JCAP* **07**, 011 (2015), [arXiv:1503.08146 \[astro-ph.CO\]](#).
- [56] A. Peimbert, M. Peimbert, and V. Luridiana, *Rev. Mex. Astron. Astrofis.* **52**, 419 (2016), [arXiv:1608.02062 \[astro-ph.CO\]](#).
- [57] R. J. Cooke, M. Pettini, and C. C. Steidel, *Astrophys. J.* **855**, 102 (2018), [arXiv:1710.11129 \[astro-ph.CO\]](#).
- [58] F. Beutler, C. Blake, M. Colless, D. H. Jones, L. Staveley-Smith, L. Campbell, Q. Parker, W. Saunders, and F. Watson, *Mon. Not. Roy. Astron. Soc.* **416**, 3017 (2011), [arXiv:1106.3366 \[astro-ph.CO\]](#).
- [59] A. J. Ross, L. Samushia, C. Howlett, W. J. Percival, A. Burden, and M. Manera, *Mon. Not. Roy. Astron. Soc.* **449**, 835 (2015), [arXiv:1409.3242 \[astro-ph.CO\]](#).

- [60] S. Alam *et al.* (BOSS), *Mon. Not. Roy. Astron. Soc.* **470**, 2617 (2017), arXiv:1607.03155 [astro-ph.CO].
- [61] A. Notari, F. Rompineve, and G. Villadoro, (2022), arXiv:2211.03799 [hep-ph].
- [62] L. Di Luzio, J. Martin Camalich, G. Martinelli, J. A. Oller, and G. Piazza, (2022), arXiv:2211.05073 [hep-ph].
- [63] E. Abdalla *et al.*, *JHEAp* **34**, 49 (2022), arXiv:2203.06142 [astro-ph.CO].
- [64] L. Perivolaropoulos and F. Skara, *New Astron. Rev.* **95**, 101659 (2022), arXiv:2105.05208 [astro-ph.CO].
- [65] E. Di Valentino, *Universe* **8**, 399 (2022).
- [66] E. Di Valentino, O. Mena, S. Pan, L. Visinelli, W. Yang, A. Melchiorri, D. F. Mota, A. G. Riess, and J. Silk, *Class. Quant. Grav.* **38**, 153001 (2021), arXiv:2103.01183 [astro-ph.CO].
- [67] S. K. Choi *et al.* (ACT), *JCAP* **12**, 045 (2020), arXiv:2007.07289 [astro-ph.CO].
- [68] S. Aiola *et al.* (ACT), *JCAP* **12**, 047 (2020), arXiv:2007.07288 [astro-ph.CO].
- [69] B. A. Benson *et al.* (SPT-3G), *Proc. SPIE Int. Soc. Opt. Eng.* **9153**, 91531P (2014), arXiv:1407.2973 [astro-ph.IM].
- [70] D. Dutcher *et al.* (SPT-3G), *Phys. Rev. D* **104**, 022003 (2021), arXiv:2101.01684 [astro-ph.CO].
- [71] E. di Valentino, S. Gariazzo, and O. Mena, *Phys. Rev. D* **106**, 043540 (2022), arXiv:2207.05167 [astro-ph.CO].
- [72] S. Gariazzo and O. Mena, *Phys. Rev. D* **99**, 021301 (2019), arXiv:1812.05449 [astro-ph.CO].
- [73] E. Di Valentino, W. Giarè, A. Melchiorri, and J. Silk, (2022), arXiv:2209.12872 [astro-ph.CO].
- [74] E. Di Valentino, W. Giarè, A. Melchiorri, and J. Silk, (2022), arXiv:2209.14054 [astro-ph.CO].
- [75] H. Jeffreys, *The Theory of Probability*, Oxford Classic Texts in the Physical Sciences (1939).
- [76] R. Trotta, *Contemp. Phys.* **49**, 71 (2008), arXiv:0803.4089 [astro-ph].
- [77] A. F. Heavens and E. Sellentin, *JCAP* **04**, 047 (2018), arXiv:1802.09450 [astro-ph.CO].
- [78] P. Stöcker *et al.* (GAMBIT Cosmology Workgroup), *Phys.Rev.* **D103**, 123508 (2021), arXiv:2009.03287 [astro-ph.CO].
- [79] L. T. Hergt, W. J. Handley, M. P. Hobson, and A. N. Lasenby, *Phys. Rev. D* **103**, 123511 (2021), arXiv:2102.11511 [astro-ph.CO].
- [80] S. Gariazzo, *Eur. Phys. J. C* **80**, 552 (2020), arXiv:1910.06646 [astro-ph.CO].
- [81] A. Lewis, A. Challinor, and A. Lasenby, *Astrophys. J.* **538**, 473 (2000), arXiv:astro-ph/9911177 [astro-ph].
- [82] C. Howlett, A. Lewis, A. Hall, and A. Challinor, *JCAP* **1204**, 027 (2012), arXiv:1201.3654 [astro-ph.CO].
- [83] K. N. Abazajian *et al.* (CMB-S4), (2016), arXiv:1610.02743 [astro-ph.CO].
- [84] W. Giarè, F. Renzi, A. Melchiorri, O. Mena, and E. Di Valentino, *Mon. Not. Roy. Astron. Soc.* **511**, 1373 (2022), arXiv:2110.00340 [astro-ph.CO].
- [85] N. Aghanim *et al.* (Planck), *Astron. Astrophys.* **641**, A6 (2020), [Erratum: *Astron. Astrophys.* 652, C4 (2021)], arXiv:1807.06209 [astro-ph.CO].
- [86] M. Forconi, W. Giarè, E. Di Valentino, and A. Melchiorri, *Phys. Rev. D* **104**, 103528 (2021), arXiv:2110.01695 [astro-ph.CO].
- [87] W. Giarè, F. Renzi, O. Mena, E. Di Valentino, and A. Melchiorri, (2022), arXiv:2210.09018 [astro-ph.CO].
- [88] W. Handley, *Phys. Rev. D* **103**, L041301 (2021), arXiv:1908.09139 [astro-ph.CO].
- [89] E. Di Valentino, A. Melchiorri, and J. Silk, *Nature Astron.* **4**, 196 (2019), arXiv:1911.02087 [astro-ph.CO].
- [90] A. Semenaite, A. G. Sánchez, A. Pezzotta, J. Hou, A. Eggemeier, M. Crocce, C. Zhao, J. R. Brownstein, G. Rossi, and D. P. Schneider, (2022), arXiv:2210.07304 [astro-ph.CO].
- [91] E. Di Valentino, A. Melchiorri, and J. Silk, *Astrophys. J. Lett.* **908**, L9 (2021), arXiv:2003.04935 [astro-ph.CO].
- [92] E. Calabrese, A. Slosar, A. Melchiorri, G. F. Smoot, and O. Zahn, *Phys. Rev. D* **77**, 123531 (2008), arXiv:0803.2309 [astro-ph].
- [93] E. Di Valentino, A. Melchiorri, and J. Silk, *JCAP* **01**, 013 (2020), arXiv:1908.01391 [astro-ph.CO].
- [94] G. Efstathiou and S. Gratton, (2019), 10.21105/astro.1910.00483, arXiv:1910.00483 [astro-ph.CO].
- [95] E. Rosenberg, S. Gratton, and G. Efstathiou, *Mon. Not. Roy. Astron. Soc.* **517**, 4620 (2022), arXiv:2205.10869 [astro-ph.CO].
- [96] A. Glanville, C. Howlett, and T. M. Davis, *Mon. Not. Roy. Astron. Soc.* **517**, 3087 (2022), arXiv:2205.05892 [astro-ph.CO].
- [97] S. Anselmi, M. F. Carney, J. T. Giblin, S. Kumar, J. B. Mertens, M. ODwyer, G. D. Starkman, and C. Tian, (2022), arXiv:2207.06547 [astro-ph.CO].
- [98] M. Chevallier and D. Polarski, *Int. J. Mod. Phys. D* **10**, 213 (2001), arXiv:gr-qc/0009008.
- [99] E. V. Linder, *Phys. Rev. Lett.* **90**, 091301 (2003), arXiv:astro-ph/0208512.
- [100] J. Torrado and A. Lewis, (2020), arXiv:2005.05290 [astro-ph.IM].
- [101] A. Lewis and S. Bridle, *Phys. Rev. D* **66**, 103511 (2002), arXiv:astro-ph/0205436.
- [102] R. M. Neal, *ArXiv Mathematics e-prints* (2005), math/0502099.
- [103] A. Heavens, Y. Fantaye, E. Sellentin, H. Eggers, Z. Hosenie, S. Kroon, and A. Mootoovaloo, *Phys. Rev. Lett.* **119**, 101301 (2017), arXiv:1704.03467 [astro-ph.CO].
- [104] A. Heavens, Y. Fantaye, A. Mootoovaloo, H. Eggers, Z. Hosenie, S. Kroon, and E. Sellentin, (2017), arXiv:1704.03472 [stat.CO].
- [105] W. J. Handley, M. P. Hobson, and A. N. Lasenby, *Mon. Not. Roy. Astron. Soc.* **450**, L61 (2015), arXiv:1502.01856 [astro-ph.CO].
- [106] W. J. Handley, M. P. Hobson, and A. N. Lasenby, *Monthly Notices of the Royal Astronomical Society* **453**, 4384 (2015), 1506.00171.
- [107] F. Simpson, R. Jimenez, C. Pena-Garay, and L. Verde, *JCAP* **06**, 029 (2017), arXiv:1703.03425 [astro-ph.CO].
- [108] T. Schwetz, K. Freese, M. Gerbino, E. Giusarma, S. Hannestad, M. Lattanzi, O. Mena, and S. Vagnozzi, (2017), arXiv:1703.04585 [astro-ph.CO].
- [109] S. Gariazzo, M. Archidiacono, P. F. de Salas, O. Mena, C. A. Ternes, and M. Törtola, *JCAP* **03**, 011 (2018), arXiv:1801.04946 [hep-ph].
- [110] P. Stöcker *et al.* (GAMBIT Cosmology Workgroup), *Phys. Rev. D* **103**, 123508 (2021), arXiv:2009.03287 [astro-ph.CO].
- [111] S. Aiola *et al.* (ACT), *JCAP* **12**, 047 (2020), arXiv:2007.07288 [astro-ph.CO].
- [112] E. Di Valentino, A. Melchiorri, and J. Silk, *Phys. Lett. B* **761**, 242 (2016), arXiv:1606.00634 [astro-ph.CO].